Effects of large bending deflections on blade flutter limits

Kallesøe, Bjarne Skovmose; Hansen, Morten Hartvig

Publication date:
2008

Document Version
Publisher's PDF, also known as Version of record

Risø-R-Report

Risø DTU
National Laboratory
for Sustainable Energy

Effects of Large Bending Deflections on Blade Flutter Limits

UpWind Deliverable D2.3

Bjarne Skovmose Kallesøe
Morten Hartvig Hansen

Risø–R–1642(EN)

UpWind

Risø National Laboratory for Sustainable Energy
Technical University of Denmark
Roskilde, Denmark
December 2008

Author: Bjarne Skovmose Kallesøe and Morten Hartvig Hansen
Title: Effects of Large Bending Deflections on Blade Flutter Limits
Department: Aeroelastic Design – Wind Energy Division

Risø–R–1642(EN)
December 2008

Abstract:
The coupling of bending and torsion due to large blade bending are assumed to have some effects of the flutter limits of wind turbines [1]. In the present report, the aeroelastic blade model suggested by Kallesøe [2], which is similar to the second order model used in [3], is used to investigate the aeroelastic stability limits of the RWT blade with and without the effects of the large blade deflection. The investigation shows no significant change of the flutter limit on the rotor speed due to the blade deflection, whereas the first edgewise bending mode becomes negatively damped due to the coupling with blade torsion which causes a change of the effective direction of blade vibration. These observations are confirmed by nonlinear aeroelastic simulations using HAWC2 [4, 5].

This work is part of the UpWind project funded by the European Commission under the contract number SES6-CT-2005-019945 which is gratefully acknowledged. This report is the deliverable D2.3 of the UpWind project.

ISSN 0106-2840

ISBN 978-87-550-3665-9

Contract no.:
SES6-CT-2005-019945

Group's own reg. no.:
1110053-01

Sponsorship:
European Commission

Cover:
UpWind logo

Pages: 12
Tables: 1
References: 8

Contents

1 Introduction

This report deals with the effects of large bending deflections under steady state operation of the wind turbine blade on its stability limits, especially with regards to the flutter limit.

Politis and Riziotis [3] have shown the importance of nonlinear effects identified by aerodynamic and aero-elastic simulations on the 5 MW Reference Wind Turbine (RWT) [8]. Their results show that the curvature of a blade with large flapwise bending under the aerodynamic loading leads to a coupling of blade torsion to the edgewise bending and loading. The blade torsion, and therefore the angle of attack along the blade, are increased near the rated speed by this coupling, which again causes the a higher thrust and mean flapwise deflections. Their aeroelastic simulations also show that the fatigue loads for blade root flapwise and edgewise moments are almost unaffected, whereas the extreme values of the torsion moment are increased.

The coupling of bending and torsion due to large blade bending are also assumed to have some effects of the flutter limits of wind turbines, as discussed in [1]. In the present report, the aeroelastic blade model suggested by Kallesøe [2], which is similar to the second order model used in [3], is used to investigate the aeroelastic stability limits of the RWT blade with and without the effects of the large blade deflection. The investigation shows no significant change of the flutter limit on the rotor speed due to the blade deflection, whereas the first edgewise bending mode becomes negatively damped due to the coupling with torsion. These observations are confirmed by nonlinear aeroelastic simulations using HAWC2 [4, 5].

To evaluate the validity of this analysis, the bending–torsion coupling due to pre-bending is investigated for a simple prebend test blade in the following subsections by computing the structural mode shapes using three different structural models.

1.1 Bending–torsion coupling due to pre-bending

The edgewise bending–torsion coupling effects of flapwise prebend on selected blade modes are investigated in this section using three different models. First, the second order Bernoulli-Euler (BE) beam theory model by Kallesøe [2] used in the subsequent flutter analysis. Second, the preliminary co-rotational finite beam element model [6] implemented in HAWCStab2 (new version of the stability tool HAWCStab [7]). Third, a solid 3D finite element model set up in the commercial tool COMSOL. Effects of the flapwise pre-bending are observed as edgewise bending–torsion coupling in the edgewise and torsional mode shapes. Qualitative agreements are seen for these effects predicted by the three different models, except that the edgewise bending component in the torsional mode is significantly smaller in the predictions by the second order BE model compared to the other two models.

1.1.1 Simple test blade

A 10 m long, prismatic, and isotropic beam is used as a test blade. The cross-section has a aspect-ratio of 2, and the height of 0.245 m is selected such that the straight beam has a natural frequency of the first flapwise bending mode of 1 Hz with $E = 50$ GN/m^2 and Poisson's ratio of 0.33 (note that the first edgewise bending mode has a natural frequency of 2 Hz). The beam has squared prebend shape with 2 m tip deflection (keeping a curve length of 10 m) as shown in Figure 1, which shows the grid of the solid 3D finite element model set up in COMSOL.

1.1.2 Comparison of mode shapes

The first ten mode shapes of the prebend test blade have been computed by all three models; however, only the first three edgewise bending modes (numbers 2, 4, and 6) and the first tor-

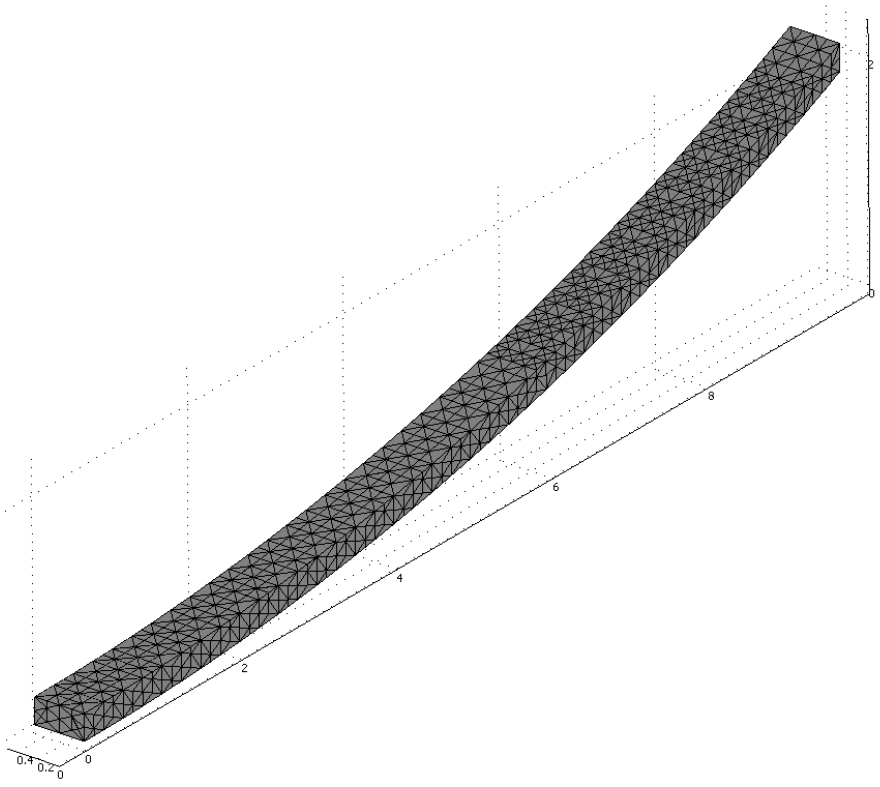

Figure 1. COMSOL model with 9,236 tetrahedral elements and 45,456 degrees of freedom which are sufficient for convergence of natural frequencies and mode shapes of the lower order modes. The 10 m test blade has squared prebend shape with 2 m tip deflection.

sional mode (number 8) are considered here, because the remaining flapwise bending modes are trivial by having no edgewise bending or torsional components in their mode shapes. The purely flapwise pre-bending of the test blade furthermore limits the comparisons of edgewise bending and torsional components, because all models agree that no flapwise bending arises due to edgewise bending or torsion of such prebend blade.

Figure 2 shows the normalized edgewise bending and torsional components in the first edgewise bending mode. The three models agree on the edgewise component, whereas the second order BE model predicts a lower torsional component than the other two models. All models agree on the qualitative behavior that the *forward* edgewise motion of a *downwind* bend blade is coupled to torsion towards *lower* angles of attack.

Figure 3 shows the normalized edgewise bending and torsional components in the second edgewise bending mode. Again, there is a qualitative agreement between the three models; note that the torsional component is most larger for the second edgewise bending mode. The co-rotational model (HAWCStab2) predicts a larger torsional component than the other two models, and the smallest torsional component is again for the second order BE model.

Figure 4 shows the computed normalized edgewise bending and torsional components in the first torsional mode. Here, the qualitative agreement is restricted to the HAWCStab2 and COMSOL predictions. There are almost no edgewise bending component in the torsional mode computed with the second order BE model. This surprising discrepancy to the other two models is still under investigation.

Figure 5 shows the computed normalized edgewise bending and torsional components in the third edgewise bending mode. Here, the qualitative (and even quantitative) agreement between the three models is restored, which eliminates higher order effects as explanation for the discrepancy for the torsional mode.

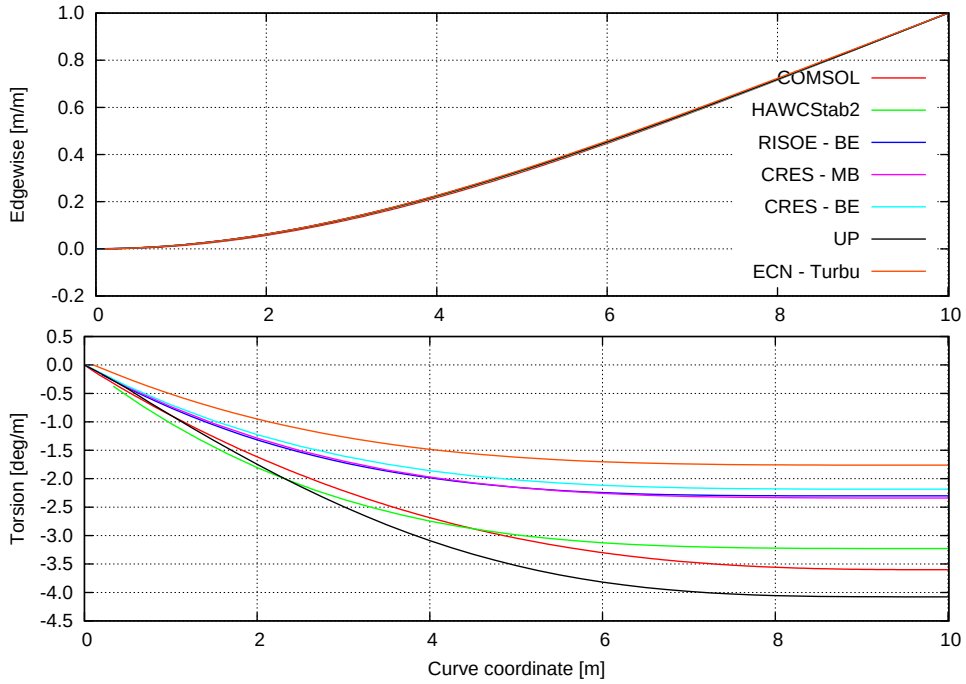

Figure 2. Edgewise bending (top) and torsional (bottom) components in the second blade mode of flapwise prebend 10 m blade computed by COMSOL model (2.02 Hz), HAWCStab2 (1.96 Hz), and second order BE model (2.02 Hz).

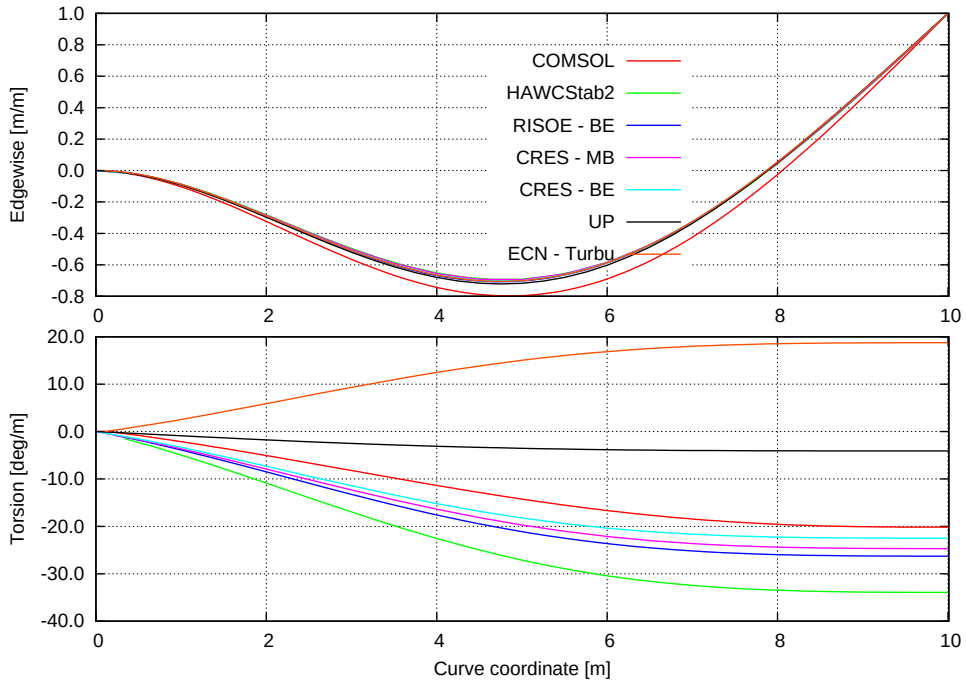

Figure 3. Edgewise bending (top) and torsional (bottom) components in the fourth blade mode of flapwise prebend 10 m blade computed by COMSOL model (11.72 Hz), HAWCStab2 (11.67 Hz), and second order BE model (12.45 Hz).

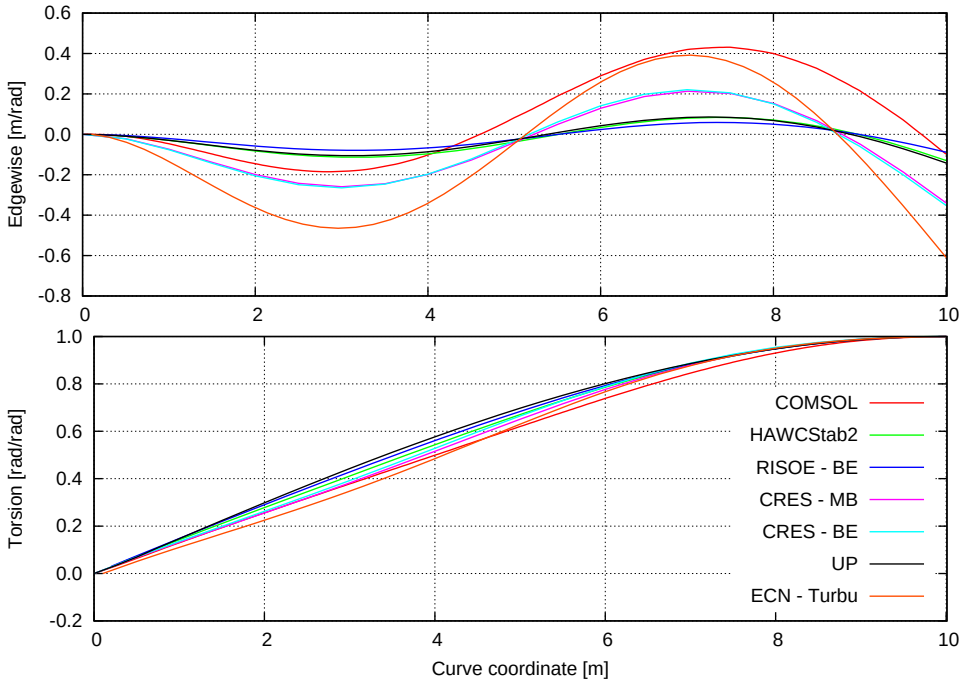

Figure 4. Edgewise bending (top) and torsional (bottom) components in the sixth blade mode of flapwise prebend 10 m blade computed by COMSOL model (29.95 Hz), HAWCStab2 (29.67 Hz), and second order BE model (31.25 Hz).

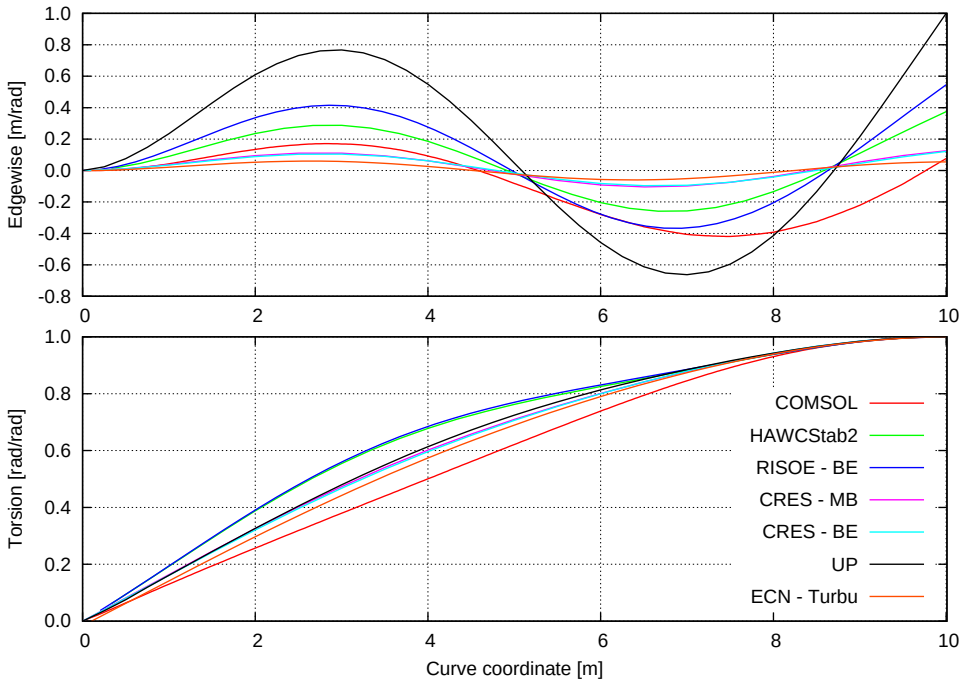

Figure 5. Edgewise bending (top) and torsional (bottom) components in the eighth blade mode of flapwise prebend 10 m blade computed by COMSOL model (35.99 Hz), HAWCStab2 (36.15 Hz), and second order BE model (34.87 Hz).

2 Stability of RWT blade

The effect of blade deflection on the aeroelastic stability is analyzed by comparing the aeroelastic modes of blade motion with and without the blade deflection due to the mean steady state aerodynamic forces. These aeroelastic modes are computed for zero pitch angle and a series of rotor speeds and corresponding wind speeds are analyzed (see Table 2). The wind speed at the different rotor speeds are chosen such that the angles of attack stay low and almost constant.

A nonlinear steady state version (no dynamic terms) of the second order Bernoulli-Euler model coupled with a Blade Element Momentum model is used to compute steady state blade deformations under the assumption of constant inflow (no shear or tower effects) and no gravity. The full dynamic nonlinear model is then linearized about this steady state deformation to form a differential eigenvalue problem, which gives the aeroelastic frequencies, damping and mode shapes for the deformed blade (see all details in [2]). Similar, the full dynamic nonlinear model is linearized about the initial blade, which leads to the aeroelastic frequencies, damping and mode shapes for the undeformed blade

To check the results of the eigenvalue analysis, the same series of rotor speeds and wind speeds are also simulated with HAWC2 [4, 5] for zero pitch angle. The damping of the least damped mode is then estimated by the exponential decay/growth of the initial blade oscillation.

2.1 Results

Figure 6 shows the tip deflection for the different operation conditions given in Table 2. The flapwise deflection become relative large for a blade length of 63 m as the rotor speed increase.

Figure 7 shows the aeroelastic frequency for the first five blade modes under the different operation conditions (Table 2) for the undeformed and deformed blade, and the dominant frequency of the transient response in the nonlinear aeroelastic simulation with HAWC2. Figure 8 shows the corresponding aeroelastic damping, except for the first and second flapwise bending modes which are highly damped and therefore not shown.

The third flapwise bending mode (the fourth mode) becomes a flutter mode around 2.35 rad/s

Rotor speed [rad/s]	Wind speed [m/s]
1.0	3.8674
1.1	4.2541
1.2	4.6409
1.3	5.0276
1.4	5.4144
1.5	5.8011
1.6	6.1878
1.7	6.5746
1.8	6.9613
1.9	7.3481
2.0	7.7348
2.1	8.1215
2.2	8.5083
2.3	8.8950
2.4	9.2818
2.5	9.6685

Table 1. Rotor speed and corresponding wind speeds used in the flutter analysis.

for both the deformed and undeformed blade. This result indicates that the large blade deflection has no significant effect on the flutter limit.

The second edgewise bending mode (the fifth mode) is significantly lower damped for the deformed blade than for the undeformed blade, which can only be explained by the increased torsional component in this edgewise bending mode due to the curvature of the flapwise blade deflection.

The first edgewise bending mode (the second mode) becomes negatively damped for rotor speeds above 1.5 rad/s when including deformations, while it stays positive damped for the undeformed blade. The HAWC2 simulations showing the dominant response (lowest damped mode) in its transients agree well with the results from the deformed blade. Notice the abrupt decrease of the damping of these transient at the rotor speed of 2.3 rad/s where the second order BE model predicts the flutter to occurs, which indicates that the HAWC2 simulations also confirms this flutter limit.

To understand the negative aeroelastic damping of the first edgewise bending mode for the deformed blade, the amplitudes and phases for the edgewise, flapwise and torsional components of this mode are plotted in Figure 9 and 10 for the undeformed and deformed blade. The phases between edgewise and flapwise blade motion are seen to shift sign for the rotor speed where the damping of the mode becomes negative. The change of sign on the phase between edgewise and flapwise blade motion corresponds to a change of the direction of vibration as shown in Figure 11. The coupling of the edgewise bending with blade torsion creates an aerodynamic coupling to between edgewise and flapwise bending through the lift–torsion coupling. The direction of vibration is related to the aerodynamic damping, and it is assumed that the negative aeroelastic damping of the first edgewise bending mode for the deformed blade is caused by this phase change.

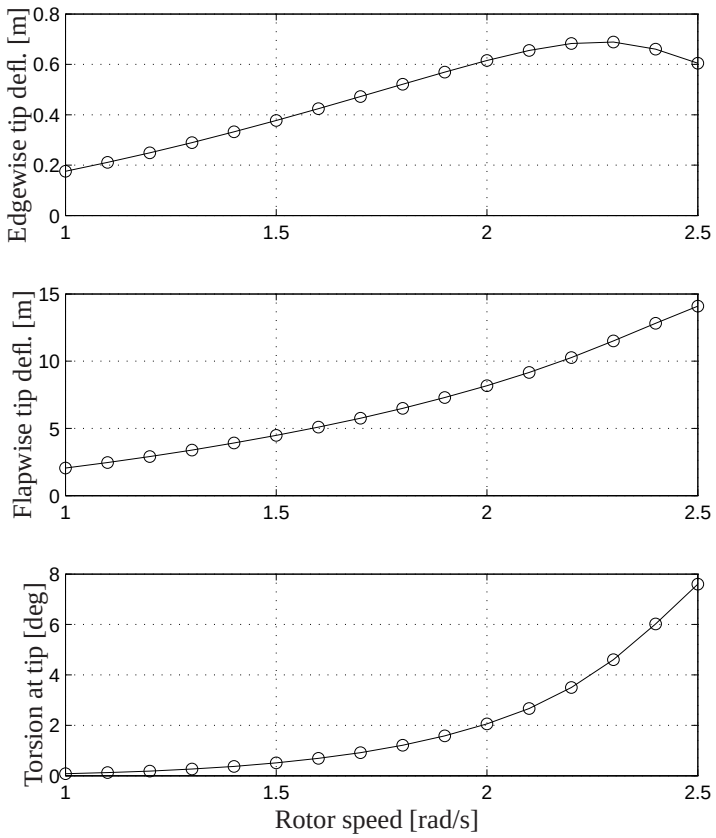

Figure 6. Tip bending deflection and torsion under steady state conditions versus rotor speed.

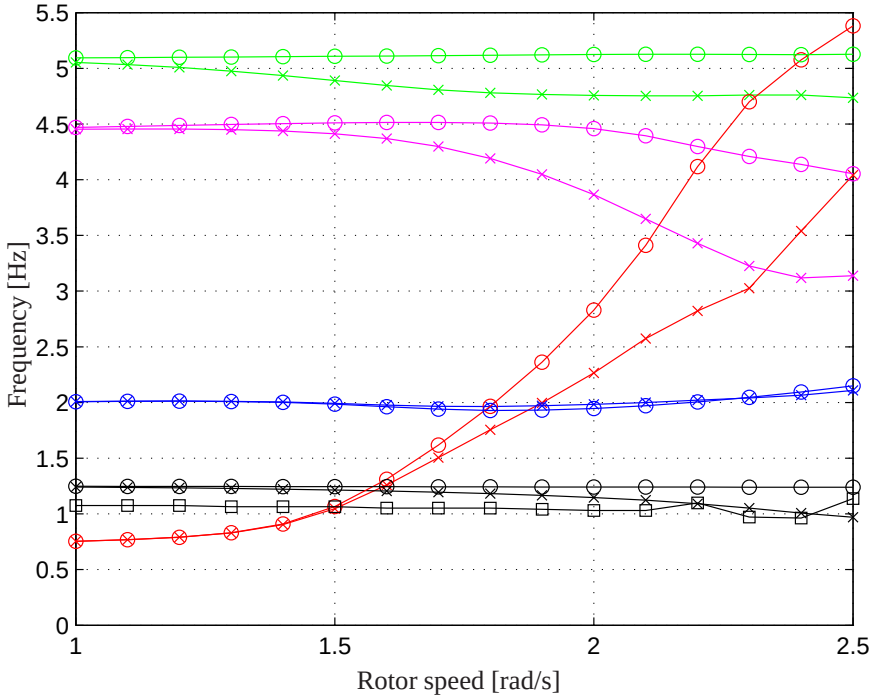

Figure 7. Aeroelastic frequencies of first flapwise (red), first edgewise (black), second flapwise (blue), third flapwise (magenta), and second edgewise (green) modes versus rotor speed. The circles (○) denote frequencies for the undeformed blade, and the crosses (×) denote results for the deformed blade. The black boxes (□) denote the dominant frequency of the transient response in the nonlinear aeroelastic simulation with HAWC2.

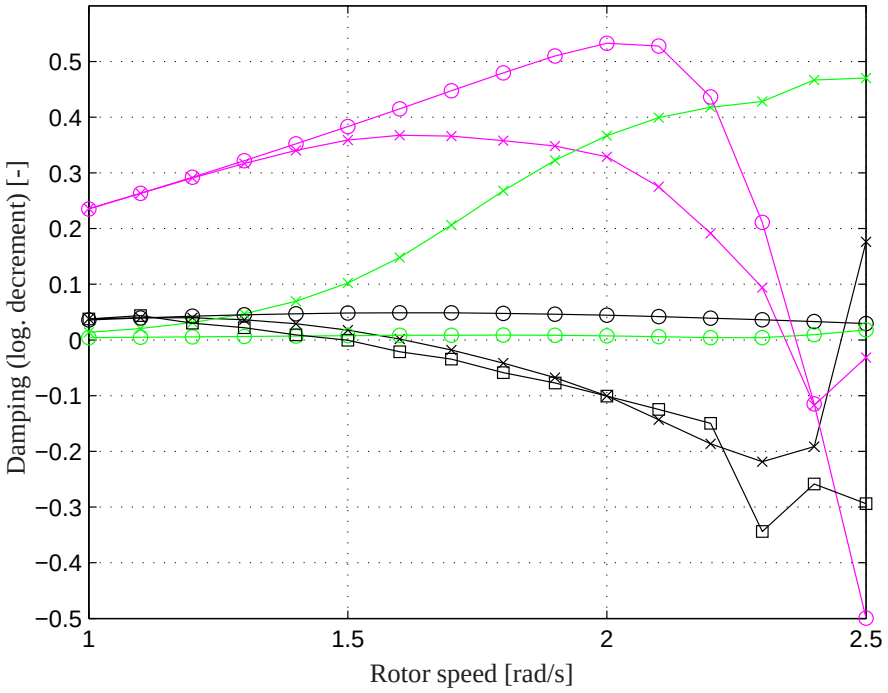

Figure 8. Aeroelastic damping of first edgewise (black), third flapwise (magenta), and second edgewise (green) modes versus rotor speed. The circles (○) denote frequencies for the undeformed blade, and the crosses (×) denote results for the deformed blade. The black boxes (□) denote the dominant frequency of the transient response in the nonlinear aeroelastic simulation with HAWC2.

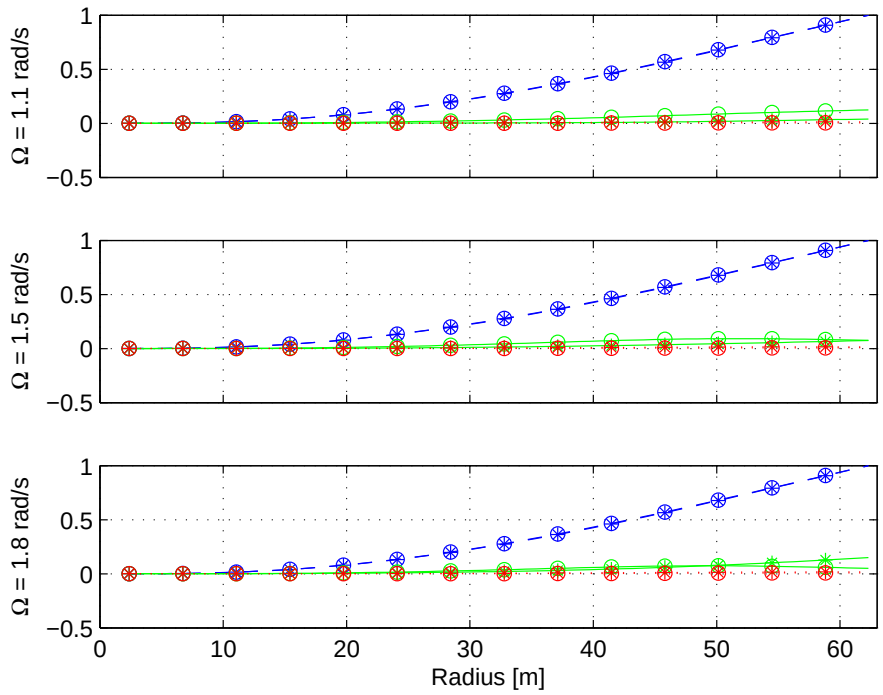

Figure 9. Amplitude of flapwise (green), edgewise (blue) and torsional (red) components of the first edgewise bending mode at different rotor speeds. Top, middle and bottom figures show the results for the rotor speeds 1.1, 1.5 and 1.8 rad/s, respectively. The circles (○) denote the components for the undeformed blade, and the crosses (×) denote the components for the deformed blade.

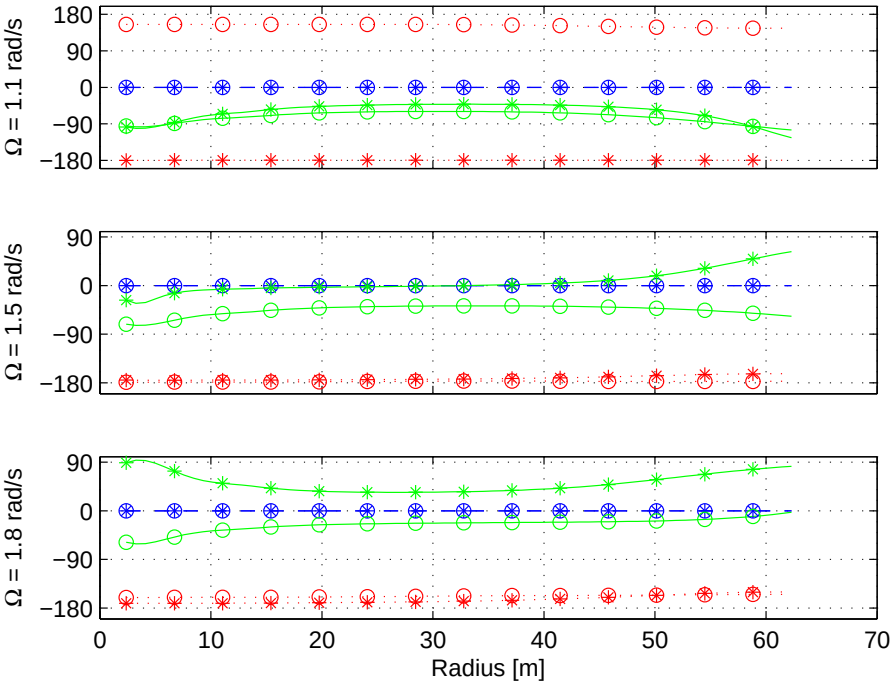

Figure 10. Phases between flapwise (green), edgewise (blue) and torsional (red) components of the first edgewise bending mode at different rotor speeds. Top, middle and bottom figures show the results for the rotor speeds 1.1, 1.5 and 1.8 rad/s, respectively. The circles (○) denote the components for the undeformed blade, and the crosses (×) denote the components for the deformed blade.

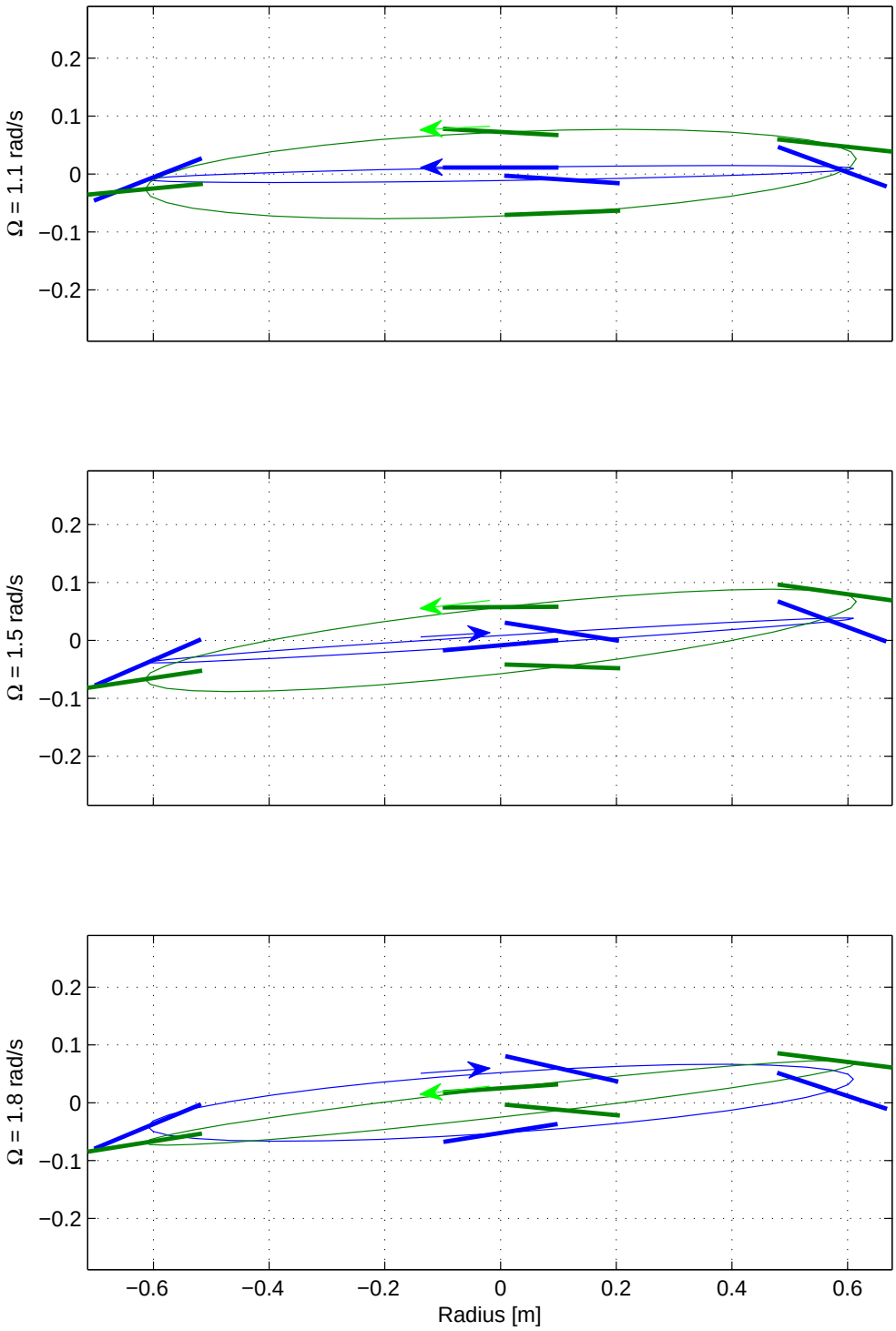

Figure 11. Traces of cross-sectional blade motion at 75 % radius in the first edgewise bending mode at different rotor speeds for the undeformed (green traces) and deformed (blue traces) blade with exaggeration of the torsional component with a factor of 1000. Arrows denote the direction of motion. Top, middle and bottom figures show the results for the rotor speeds 1.1, 1.5 and 1.8 rad/s, respectively. Note that the relative wind becomes from right to left in the displayed cross-sectional coordinate system.

3 Conclusion

This report deals with the effects of large bending deflections under steady state operation of the wind turbine blade on its stability limits, especially with regards to the flutter limit. The coupling of bending and torsion due to large blade bending are assumed to have some effects of the flutter limits of wind turbines [1]. In the present report, the aeroelastic blade model suggested by Kallesøe [2], which is similar to the second order model used in [3], is used to investigate the aeroelastic stability limits of the RWT blade with and without the effects of the large blade deflection. The investigation shows no significant change of the flutter limit on the rotor speed due to the blade deflection, whereas the first edgewise bending mode becomes negatively damped due to the coupling with blade torsion which causes a change of the effective direction of blade vibration. These observations are confirmed by nonlinear aeroelastic simulations using HAWC2 [4, 5].

This work is part of the UpWind project funded by the European Commission under the contract number SES6-CT-2005-019945 which is gratefully acknowledged. This report is the deliverable D2.3 of the UpWind project. The present results will be follow up by a more detailed report including the results from other partners on the aeroelastic stability of the RWT blade with large bending deflection.

References

[1] M. H. Hansen. Aeroelastic instability problems for wind turbines. *Wind Energy*, 10:551–577, 2007.

[2] B. S. Kallesøe. Equations of motion for a rotor blade, including gravity, pitch action and rotor speed variations. *Wind Energy*, 10:209–230, 2007.

[3] E. Politis and V. Riziotis. The importance of nonlinear effects identified by aerodynamic and aero-elastic simulations on the 5 mw reference wind turbine. Deliverable D2.1, Project UpWind, September 2007. (Restricted to WP members).

[4] T. J. Larsen, A. M. Hansen, and T. Buhl. Aeroelastic effects of large blade deflections for wind turbines. In *Proceedings of The Science of Making Torque from Wind*, pages 238–246, The Netherlands, April 2004. Delft University of Technology.

[5] T. J. Larsen, H. Aa. Madsen, A. M. Hansen, and K. Thomsen. Investigations of stability effects of an offshore wind turbine using the new aeroelastic code HAWC2. *Proceedings of the conference "Copenhagen Offshore Wind 2005"*, 2005.

[6] M. A. Crisfield. *Non-linear Finite Element Analysis of Solids and Structures*, volume 2. Wiley, New York, 1997.

[7] M. H. Hansen. Aeroelastic stability analysis of wind turbines using an eigenvalue approach. *Wind Energy*, 7:133–143, 2004.

[8] J. Jonkman. NREL 5 MW baseline wind turbine. Technical report, NREL/NWTC, 1617 Cole Boulevard; Golden, CO 80401-3393, USA, 2005.